Supplementary Material

HGD-derived *N*-formylkynurenine promotes small cell lung cancer chemoresistance by activating ATL2-mediated endoplasmic reticulum remodelling

Ruibin Yi[1,#], Yueming Zhang[1,#], Jiayi Cai[1], Qingxi Zhang[2], Haoxuan Ying[1], Ting Wei[1,*], Jian Zhang[1,*], Weitao Shen[1,*]

Affiliations

[1] Department of Oncology, Zhujiang Hospital, Southern Medical University, Guangzhou, Guangdong, 510280, China.

[2] Department of Rehabilitation Medicine, The Second Affiliated Hospital, Guangzhou Medical University, Guangzhou, China.

* Correspondence: Weitao Shen, M.D., Ph.D., Department of Oncology, Zhujiang Hospital, Southern Medical University. Email: shenweitao1@i.smu.edu.cn

Jian Zhang, M.D., Ph.D., email: zhangjian@i.smu.edu.cn

Ting Wei, M.D., Ph.D., email: weitingyouyou@qq.com

[#] Contributed equally.

Extended Data Fig. 1

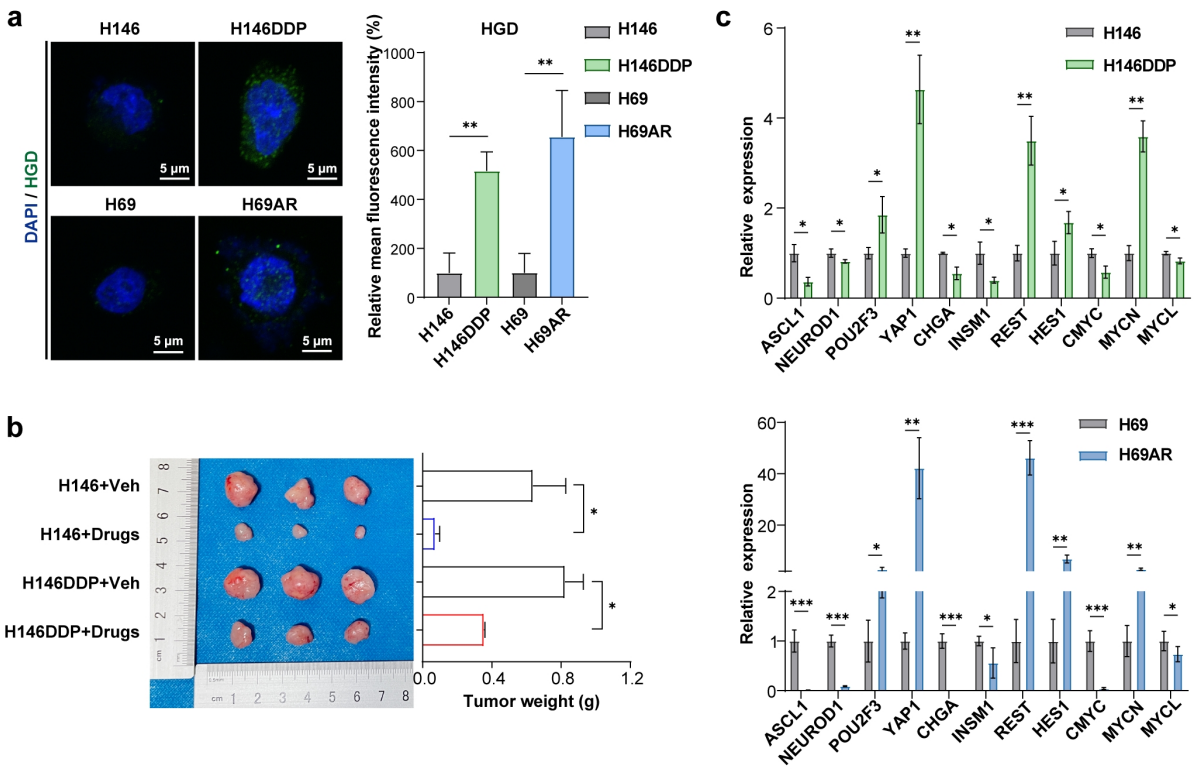

Extended Data Fig. 1, related to Fig. 1.

a, Immunofluorescence staining of HGD (green) and nuclei (DAPI, blue) in parental and chemoresistant SCLC cell lines, with quantification (right) showing higher cytoplasmic HGD fluorescence in chemoresistant cells. Scale bars, 5 μm. Representative images of n = 3 biological replicates. **b,** Representative images of xenograft tumours and the corresponding tumour burdens derived from parental H146 and chemoresistant H146DDP cells treated with vehicle (Veh) or cisplatin plus etoposide (Drugs). n = 3. **c,** Relative mRNA expression of neuroendocrine (NE) markers in parental (H146 and H69) and chemoresistant (H146DDP and H69AR) SCLC cells. Chemoresistant cells exhibit increased expression of non-NE markers (YAP1, REST, and HES1) and reduced expression of NE markers (ASCL1, NEUROD1, CHGA, and INSM1). n = 3.

Data are presented as the mean ± s.d. Statistical analysis was performed using two-tailed unpaired Student's t test (**a, c**), or unpaired t test with Welch's correction (**b**). **P* < 0.05, ***P* < 0.01, ****P* < 0.001, *****P* < 0.0001.

Extended Data Fig. 2

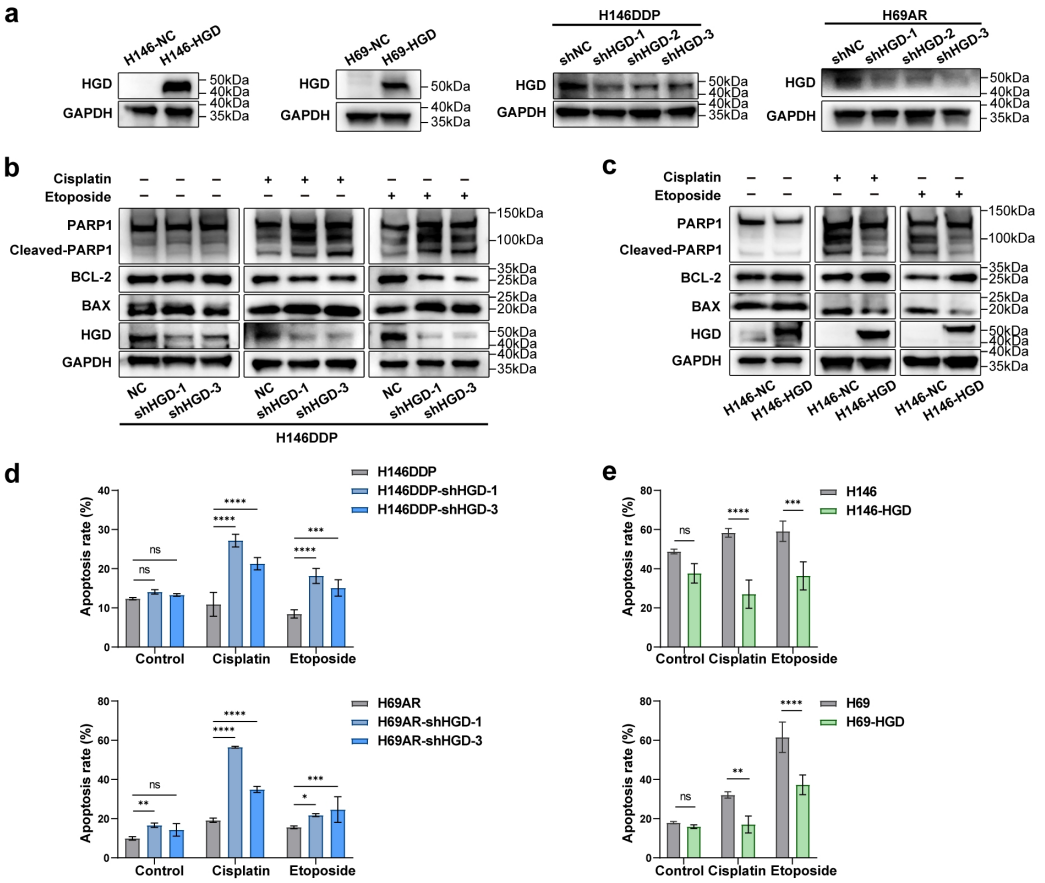

Extended Data Fig. 2, related to Fig. 2.

a, Immunoblot analysis confirming HGD overexpression in H146 and H69 cells and HGD knockdown in H146DDP and H69AR cells. Representative images of n = 3 biological replicates. **b, c,** Immunoblot analysis of PARP1, cleaved PARP1, BCL-2, and BAX expression in H146DDP cells with NC or HGD knockdown **(b)** and in H146 cells with NC or HGD overexpression **(c)** following treatment with cisplatin or etoposide. Representative images of n = 3 biological replicates. **d, e,** Quantification of apoptosis by flow cytometry in H146DDP and H69AR cells with or without HGD knockdown **(d)** and in H146 and H69 cells with NC with or without HGD overexpression **(e)** following treatment with cisplatin or etoposide. n = 3.

The data are presented as mean ± SD. Statistical analysis was performed using two-way ANOVA with Sidak's multiple-comparison test **(d, e)**. ns, not significant; **P*<0.05, ***P* < 0.01, ****P* < 0.001, *****P* < 0.0001.

Extended Data Fig. 3

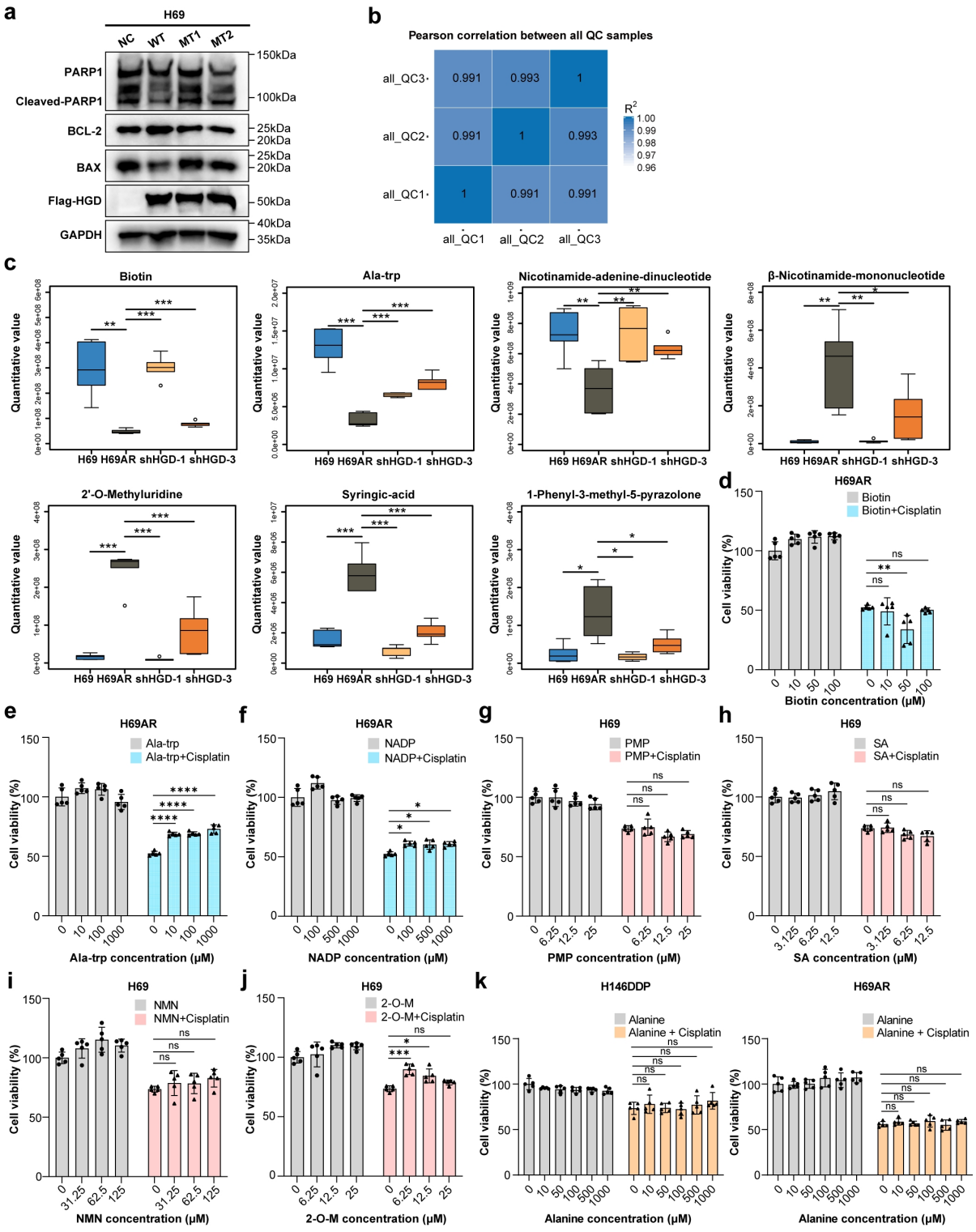

Extended Data Fig. 3, related to Fig. 3.

a, Immunoblot analysis of PARP1, cleaved PARP1, BCL-2, BAX, and Flag-HGD expression in H69 cells expressing control vector (NC), wild-type HGD (WT), or

catalytically impaired mutants (MT1, R225H; or MT2, I216T) following cisplatin treatment. Representative images of n = 3 biological replicates. **b,** Pearson correlation matrix of quality control (QC) samples from the untargeted metabolomics dataset. n = 6. **c,** Quantification of selected metabolites identified in **Fig. 3 (e)**, including biotin, nicotinamide adenine dinucleotide (NADP), β-nicotinamide mononucleotide (NMN), 2'-O-methyluridine, syringic acid, and 1-phenyl-3-methyl-5-pyrazolone (PMP), in H69, H69AR, and H69AR cells with HGD knockdown. n = 6.

d–f, Viability of H69AR cells treated with increasing concentrations of biotin **(d)**, Ala-Trp **(e)** or NADP **(f)** with or without cisplatin. n = 5. The 0 μM conditions (with or without cisplatin) represent untreated baseline controls measured once within the same experimental run; hence, the same control values are shared across panels **(d–f)** to ensure internal consistency. **g–j,** Viability of H69 cells treated with PMP **(g)**, syringic acid **(h)**, NMN **(i)** or 2-O-M **(j)** with or without cisplatin. n = 5. The 0 μM groups (with or without cisplatin) correspond to common baseline controls acquired in the same experiment and are therefore shared across panels **(g-j)**. **k,** Viability of H146DDP and H69AR cells treated with alanine with or without cisplatin. n = 5.

Data are presented as the mean ± s.d. Statistical analysis was performed using two-tailed unpaired Student's t test **(c)** or two-way ANOVA with Sidak's multiple-comparison test **(d-k)**. ns, not significant; **P* < 0.05, ***P* < 0.01, ****P* < 0.001, *****P* < 0.0001.

Extended Data Fig. 4

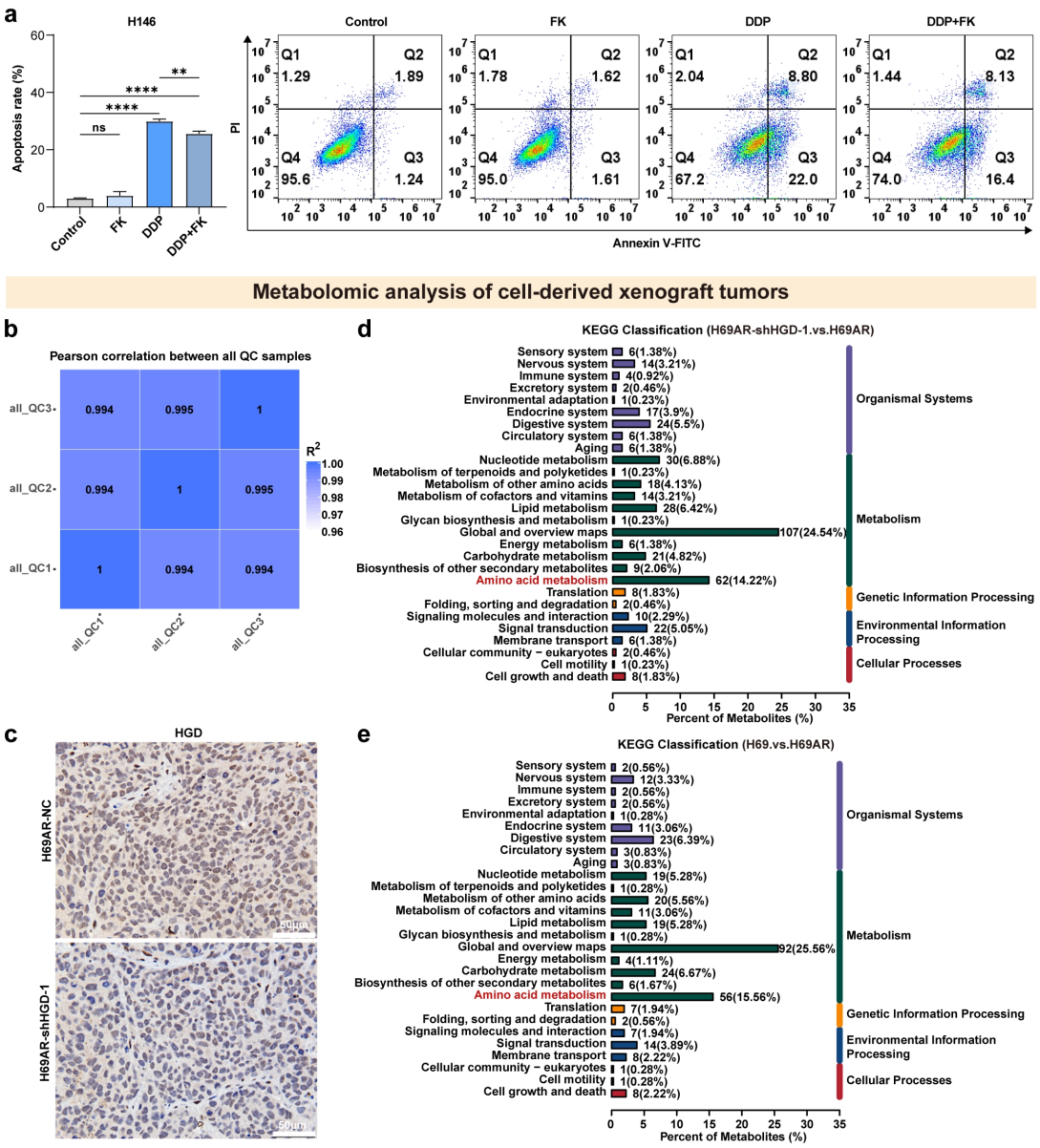

Extended Data Fig. 4, related to Fig. 4.

a, Flow cytometry analysis and quantification of apoptosis in H146 cells treated with *N*-formylkynurenine (FK), cisplatin (DDP), or their combination. n = 3. Data are presented as the mean ± s.d. Statistical analysis was performed using one-way ANOVA with Sidak's multiple-comparison test. ns, not significant, $^{**}P < 0.01$, $^{****}P < 0.0001$. **b,** Pearson correlation matrix of quality-control (QC) samples from the untargeted metabolomic profiling of xenograft tumours. n = 6. **c,** Representative immunohistochemistry images of HGD in xenograft tumours derived from H69AR-NC and H69AR-shHGD-1 cells. Scale

bars, 50 μm. **d, e,** KEGG functional classification of differentially abundant metabolites in H69AR-shHGD-1 versus H69AR-NC xenograft tumours **(d)** and H69 versus H69AR xenograft tumours **(e)**. n = 6.

Extended Data Fig. 5

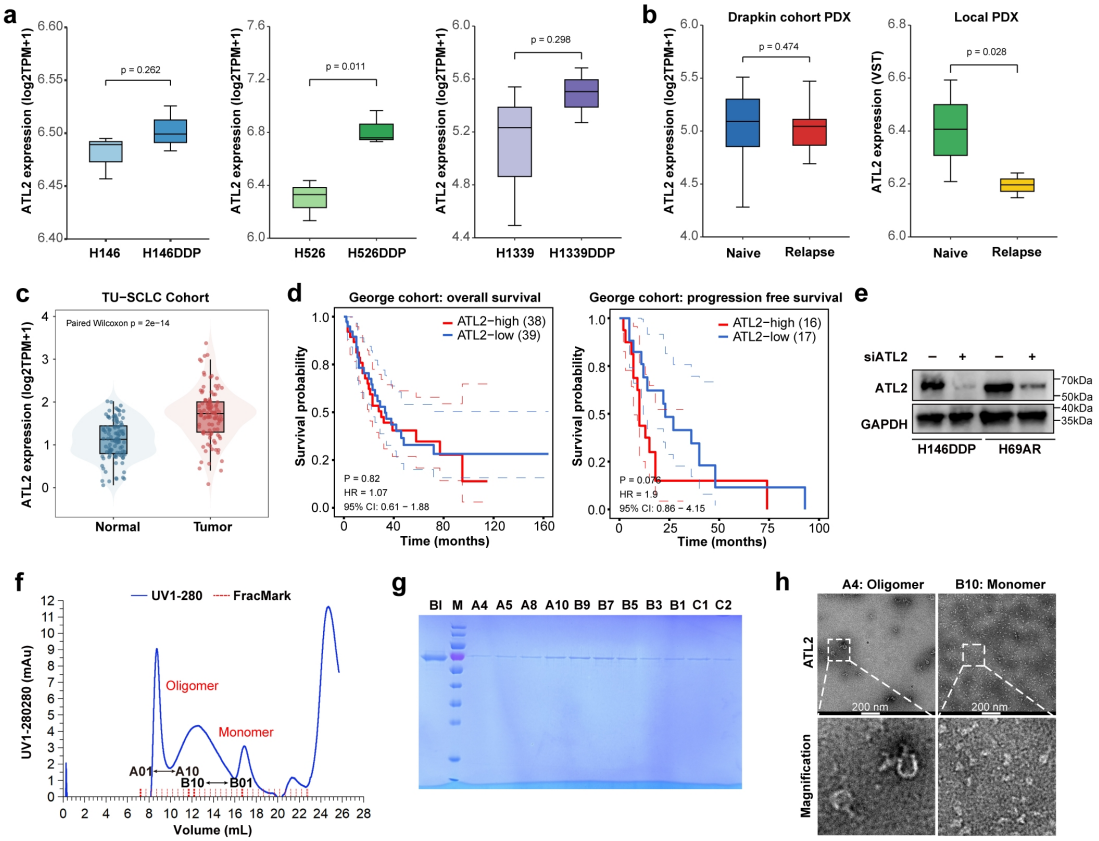

Extended Data Fig. 5, related to Fig. 6.

a, Boxplots showing ATL2 mRNA expression (log2TPM) in chemotherapy-sensitive and chemotherapy-resistant SCLC cell line pairs (H146/H146DDP, H526/H526DDP, and H1339/H1339DDP). **b,** ATL2 expression levels in naive versus relapsed PDX tumours from the Drapkin cohort (left) and the local PDX cohort (right). **c,** Paired ATL2 expression in matched normal lung and tumour tissues from the TU-SCLC cohort (n paired samples = 174). **d,** Kaplan–Meier curves of overall survival (left) and progression-free survival (right) in the George cohort stratified by ATL2 expression. **e,** Immunoblot analysis showing the efficiency of ATL2 knockdown in chemoresistant SCLC cells (H146DDP and H69) transfected with siATL2. Representative blots of n = 3 biological replicates. **f**, Size-exclusion chromatography (SEC) profiles of the purified recombinant ATL2 protein showing monomeric and oligomeric peaks (UV absorbance at 280 nm). The fraction index is annotated (FracMark). **g**, SDS–PAGE analysis of sequential SEC fractions corresponding to oligomeric (A4-A10) and monomeric (B1-B10) ATL2 species. BI and M

represent the input before SEC and the molecular weight marker, respectively. **h**, Negative stain transmission electron microscopy images of SEC-purified ATL2 monomeric and oligomeric fractions (examples: A4, B1, and B10). Scale bars, 50 nm.

Statistical analysis was performed using two-tailed unpaired Student's t test **(a),** unpaired t test with Welch's correction **(b)**, or two-tailed paired Student's t test **(c)**.

Extended Data Fig. 6

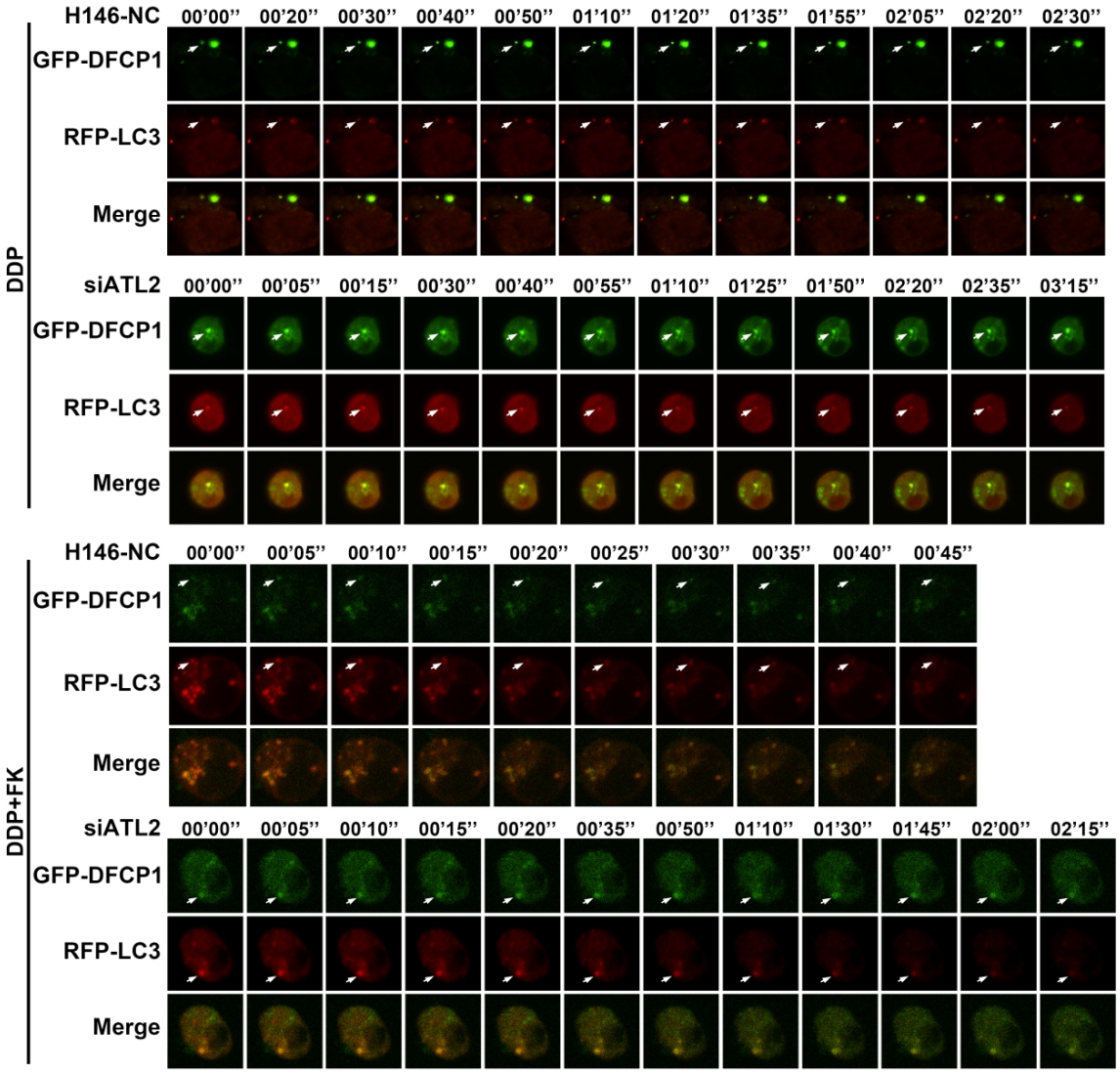

Extended Data Fig. 6, related to Fig. 7.

Time-lapse confocal images of H146 cells coexpressing GFP-DFCP1 and RFP-LC3 after cisplatin (DDP) treatment with or without FK (100 μM) in the presence of control siRNA or ATL2-siRNA. White arrowheads indicate LC3 puncta that transiently colocalized with DFCP1-positive ER subdomains. Time stamps denote the interval from LC3 appearance on the ER to its disappearance.

Extended Data Fig. 7

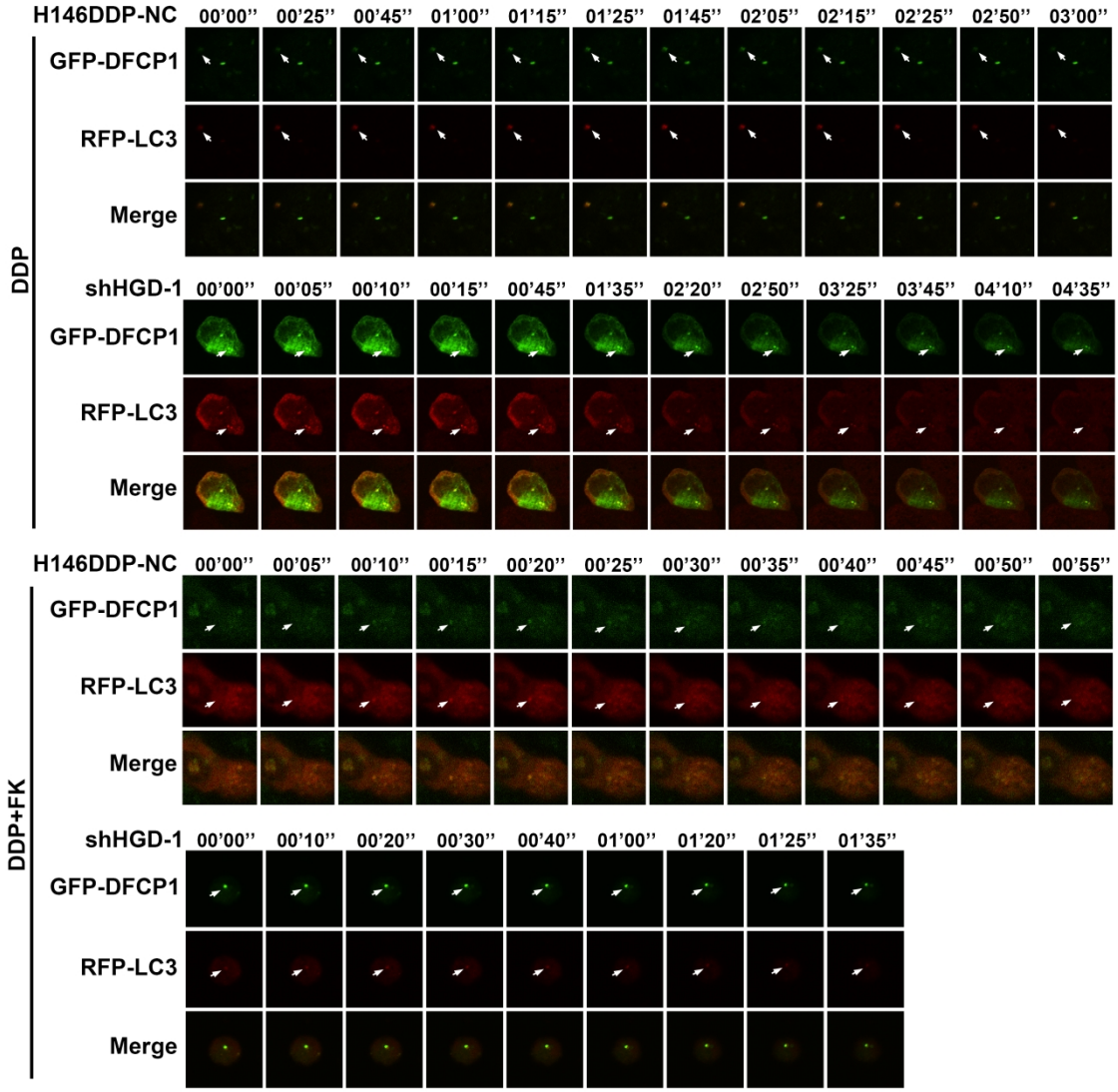

Extended Data Fig. 7, related to Fig. 7.

Time-lapse confocal images of H146DDP cells coexpressing GFP-DFCP1 and RFP-LC3 following treatment with cisplatin (DDP) or DDP/FK with or without HGD knockdown. White arrowheads indicate LC3 puncta that transiently colocalized with DFCP1-positive ER subdomains. Time stamps denote the interval from LC3 appearance on the ER to its disappearance.

Extended Data Fig. 8

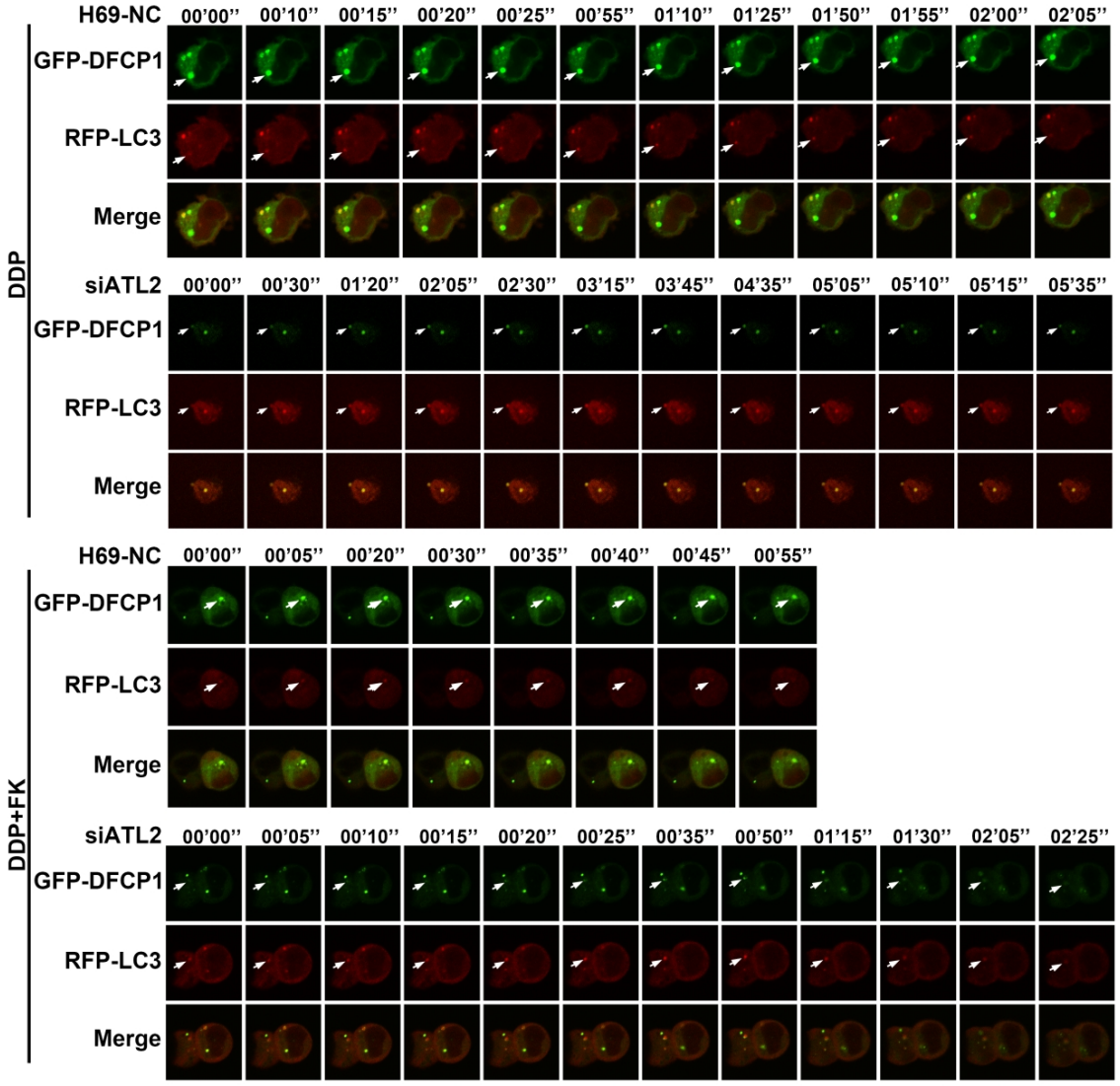

Extended Data Fig. 8, related to Fig. 7.

Time-lapse confocal images of H69 cells coexpressing GFP-DFCP1 and RFP-LC3 after cisplatin (DDP) treatment with or without FK (100 μM) in the presence of control siRNA or ATL2-siRNA. White arrowheads indicate LC3 puncta that transiently colocalized with DFCP1-positive ER subdomains. Time stamps denote the interval from LC3 appearance on the ER to its disappearance.

Extended Data Fig. 9

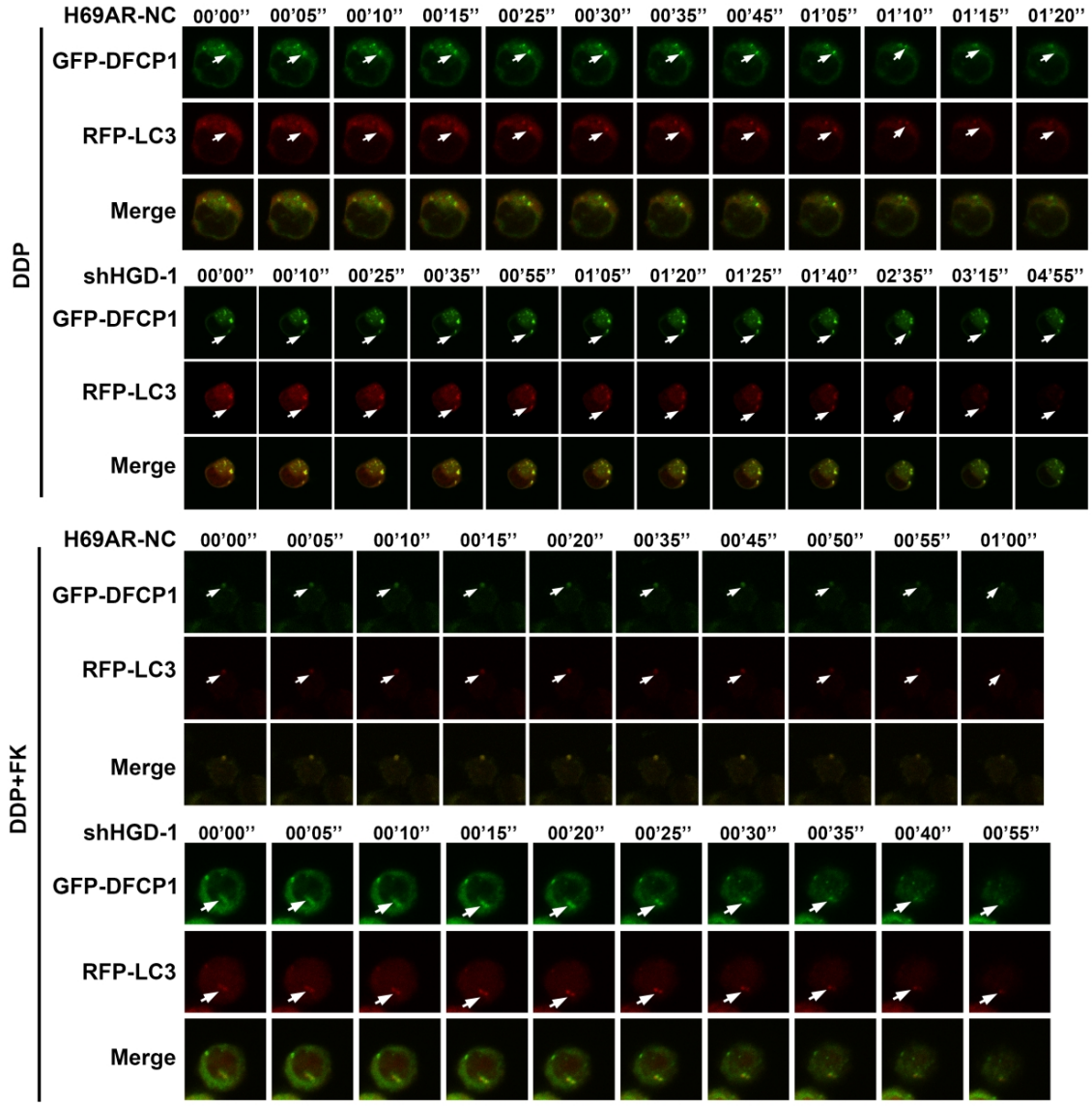

Extended Data Fig. 9, related to Fig. 7.

Time-lapse confocal images of H69AR cells coexpressing GFP-DFCP1 and RFP-LC3 following treatment with cisplatin (DDP) or DDP/FK with or without HGD knockdown. White arrowheads indicate LC3 puncta that transiently colocalized with DFCP1-positive ER subdomains. Time stamps denote the interval from LC3 appearance on the ER to its disappearance.